Melts of semiflexible diblock copolymer

M. W. Matsen
Department of Chemical Engineering and Materials Science, University of Minnesota, Minneapolis, Minnesota 55455

(Received 14 November 1995; accepted 14 February 1996)

Melts of semiflexible AB diblock copolymers are studied using the wormlike chain model and self-consistent-field theory. The diblocks considered here are symmetric in composition and in A- and B-block flexibility. Under these conditions, the microstructure formed is lamellar. We find that an increase in molecular rigidity moves the order–disorder transition from $\chi N=10.495$ for Gaussian chains to $\chi N=6.135$ for rigid rods. In the ordered state, rigidity has little effect on the exponents that describe the scaling of the domain spacing and of the interfacial width with molecular weight. However, the proportionality constants are significantly affected. The spatial and orientational distribution of segments in the ordered microstructure is examined for a selection of conditions. © *1996 American Institute of Physics.* [S0021-9606(96)50219-6]

I. INTRODUCTION

Over the past couple decades, experiments have revealed that block copolymer melts exhibit a geometrically rich selection of microstructures.[1] Recently, it has been illustrated that self-consistent-field theory (SCFT)[2] models this block copolymer phase behavior rather well.[3] An appealing aspect of the theory is that the model upon which it is based is inherently simple and intuitive. It accounts for the hard-core interactions between molecules by implementing an incompressibility constraint, and treats the attractive interactions, which lead to immiscibility between unlike segments, by a simple Flory–Huggins interaction term with a strength controlled by one parameter χ. The individual polymers are assumed to be completely flexible Gaussian chains. It has already been established that fluctuations[4] can explain most of the differences between this SCFT and experiment, occurring in the vicinity of the order–disorder transition (ODT). Presumably, the remaining differences can be explained with small refinements to the model by including, for example, finite compressibility effects, a more accurate enthalpy term, and rigidity in the polymer chains.

Here, we address the effects of molecular rigidity.[5] This can be done within the SCFT by replacing the statistical weight assigned to the space curve of a polymer molecule from that of a Gaussian chain to that of a wormlike chain.[6] In the Gaussian model, the weight assigned to the configuration of a molecule depends upon the degree to which the individual segments are stretched. This weighting is controlled by a single parameter, the statistical segment length a. The wormlike model[7] constrains segments to a constant contour length, b, and weights the configuration based on the curvature of the segments and a dimensionless bending modulus, κ. In this model, the statistical segment length is $a=b(2\kappa)^{1/2}$. When a polymer of N segments has a persistence length, $\xi=b\kappa$, much smaller than its contour length, bN, and the fields acting on it vary slowly over distances of order ξ, then the wormlike model reduces to the Gaussian one.[6,8]

Even in the limit of high molecular weight (i.e., $N\gg\kappa$), a finite rigidity can affect an ordered microstructure provided ξ is comparable to the width w of its internal interface. For strongly segregated flexible block copolymers, the width is approximately $w_0 = 2a(6\chi)^{-1/2} = 2b(\kappa/3\chi)^{1/2}$.[9] Therefore, $\xi/w_0 \propto (\kappa\chi)^{1/2}$ and molecular rigidity effects are controlled by the product $\kappa\chi$. When $\kappa\chi\ll 1$, the Gaussian model remains accurate, but when $\kappa\chi\sim 1$, molecular rigidity affects the internal interface of the microstructure. Because microphase separation involves a competition between interfacial tension and entropic stretching energy of the molecules, phase behavior may be altered. At high degrees of rigidity (i.e., $\kappa\gtrsim N$), ξ becomes comparable to the domain spacing D, and polymeric behavior crosses over to that of liquid crystals. In this limit, packing frustration will dominate phase behavior and presumably complex phases will be suppressed in favor of layered phases (i.e., thermotropic liquid crystals). Naturally, selective solvents could be used to relieve this frustration, again stabilizing the complex phases (i.e., lyotropic liquid crystals).

Below, we begin by formulating the SCFT for melts of wormlike diblock copolymers. Then, the theory is applied to a representative microstructure, the lamellar phase. The effect of molecular rigidity on the order–disorder transition is determined. In the ordered state, domain sizes and interfacial widths are examined. The study concludes with an examination of segment distributions in strongly segregated lamellar microstructures.

II. THEORY

We consider a monodisperse melt of n AB diblock copolymers. Each molecule is composed of N segments where a fraction f forms the A block and the remaining forms the B block. Both A and B segments are assumed to be incompressible and defined to have the same volume, $1/\rho_0$. The total volume of the system is $V=nN/\rho_0$. The space curve of the α'th molecule is specified by $\mathbf{r}_\alpha(s)$, where s is a parameter that varies continuously along its contour: $s=0$ at the A end, $s=f$ at the junction, and $s=1$ at the B end.

The procedure for calculating the free energy of a melt

 0021-9606/96/104(19)/7758/7/$10.00

of wormlike chains closely parallels that given in Ref. 10 for Gaussian chains. The partition function takes the same form

$$Z=\int\left(\prod_{\alpha=1}^{n}\mathscr{D}\mathbf{r}_\alpha P[\mathbf{r}_\alpha;0,1]\right)\delta[1-\hat{\phi}_A-\hat{\phi}_B]\times\exp\left\{-\chi\rho_0\int d\mathbf{r}\;\hat{\phi}_A(\mathbf{r})\hat{\phi}_B(\mathbf{r})\right\} \tag{1}$$

except that the space curves are now weighted by a new functional[6,8,11]

$$P[\mathbf{r}_\alpha;s_1,s_2]\propto\delta[1-|\mathbf{u}_\alpha|]\times\exp\left\{-\frac{\kappa}{2N}\int_{s_1}^{s_2}ds\left|\frac{d}{ds}\mathbf{u}_\alpha(s)\right|^2\right\}, \tag{2}$$

where

$$\mathbf{u}_\alpha(s)\equiv\frac{1}{bN}\frac{d}{ds}\mathbf{r}_\alpha(s). \tag{3}$$

The delta functional in Eq. (2) ensures that $\mathbf{u}_\alpha(s)$ is a unit vector, which in turn ensures that each segment has a fixed contour length b. The bending rigidity of the segments is controlled by κ. We restrict the present study to the case where A and B segments have identical lengths and flexibility, although the extension to unequal b and κ is straightforward. The Flory–Huggins parameter, χ, measures the incompatibility between A and B segments. The dimensionless A-segment-density operator in Eq. (1) is given by

$$\hat{\phi}_A(\mathbf{r})=\frac{N}{\rho_0}\sum_{\alpha=1}^{n}\int_0^f ds\,\delta(\mathbf{r}-\mathbf{r}_\alpha(s)), \tag{4}$$

and $\hat{\phi}_B(\mathbf{r})$ is given by an analogous expression.

As in Ref. 10, steps are taken to make the expression for Z more manageable. A functional integral, $1=\int\mathscr{D}\Phi_A\delta[\Phi_A-\hat{\phi}_A]$, is inserted, which permits the replacement of the operator $\hat{\phi}_A$ by the function Φ_A. The same is done for $\hat{\phi}_B$, and then the delta functionals are replaced by standard integral representations. This transforms Eq. (1) into

$$Z=\mathscr{N}\int\mathscr{D}\Phi_A\mathscr{D}W_A\mathscr{D}\Phi_B\mathscr{D}W_B\mathscr{D}\Xi\exp\{-F/k_BT\}, \tag{5}$$

where $\mathscr{N}$ is a normalization constant,

$$\frac{F}{nk_BT}\equiv-\ln\mathscr{Q}+V^{-1}\int d\mathbf{r}\{\chi N\Phi_A(\mathbf{r})\Phi_B(\mathbf{r})-W_A(\mathbf{r})\Phi_A(\mathbf{r})-W_B(\mathbf{r})\Phi_B(\mathbf{r})-\Xi(\mathbf{r})\times[1-\Phi_A(\mathbf{r})-\Phi_B(\mathbf{r})]\}, \tag{6}$$

$$\mathscr{Q}\equiv\int\mathscr{D}\mathbf{r}_\alpha P[\mathbf{r}_\alpha;0,1]\exp\left\{-\int_0^f ds\,W_A(\mathbf{r}_\alpha(s))-\int_f^1 ds\,W_B(\mathbf{r}_\alpha(s))\right\}. \tag{7}$$

Because the functional integral in Eq. (5) cannot be evaluated, it is approximated by the extremum of the integrand. This is the mean-field approximation and it estimates the free energy, $-k_BT\ln Z$, by $F[\phi_A,w_A,\phi_B,w_B,\xi]$, where ϕ_A, w_A, ϕ_B, w_B, and ξ are the functions for which F attains its minimum. Requiring variations in F with respect to each of its five functions to be zero,

$$\phi_A=-\frac{V}{\mathscr{Q}}\frac{\mathscr{D}\mathscr{Q}}{\mathscr{D}w_A}, \tag{8}$$

$$\phi_B=-\frac{V}{\mathscr{Q}}\frac{\mathscr{D}\mathscr{Q}}{\mathscr{D}w_B}, \tag{9}$$

$$\phi_A(\mathbf{r})+\phi_B(\mathbf{r})=1, \tag{10}$$

$$w_A(\mathbf{r})=\chi N\phi_B(\mathbf{r})+\xi(\mathbf{r}), \tag{11}$$

$$w_B(\mathbf{r})=\chi N\phi_A(\mathbf{r})+\xi(\mathbf{r}). \tag{12}$$

Noting that $\mathscr{Q}[w_A,w_B]$ is the partition function for a diblock with A and B segments subject to fields, $w_A(\mathbf{r})$ and $w_B(\mathbf{r})$, respectively, identifies $\phi_A(\mathbf{r})$ as the average A-segment density. Likewise, $\phi_B(\mathbf{r})$ is the average B-segment density. It then follows that Eq. (10) is the incompressibility constraint. Equations (11) and (12) are the self-consistent equations corresponding to the two fields.

In order to solve the set of equations (8)–(12), it is necessary to first evaluate the partition function, $\mathscr{Q}[w_A,w_B]$. To do this, we express it as $\mathscr{Q}=\int d\mathbf{r}d\mathbf{u}q(\mathbf{r},\mathbf{u},1)$, where

$$q(\mathbf{r},\mathbf{u},s)=\int\mathscr{D}\mathbf{r}_\alpha P[\mathbf{r}_\alpha;0,s]\delta(\mathbf{r}-\mathbf{r}_\alpha(s))\,\delta(\mathbf{u}-\mathbf{u}_\alpha(s))\times\exp\left\{-\int_0^s dt[\gamma(t)w_A(\mathbf{r}_\alpha(t))+(1-\gamma(t))w_B(\mathbf{r}_\alpha(t))]\right\} \tag{13}$$

is an end-segment distribution function. [$\gamma(t)$ is a step function that is 1 for $t<f$ and 0 otherwise.] This distribution function satisfies

$$\frac{\partial q}{\partial s}+bN\mathbf{u}\cdot\nabla_r q=\begin{cases}\dfrac{N}{2\kappa}\nabla_u^2 q-w_A(\mathbf{r})q, & \text{if } s<f,\\[2ex] \dfrac{N}{2\kappa}\nabla_u^2 q-w_B(\mathbf{r})q, & \text{if } f<s,\end{cases} \tag{14}$$

and the initial condition, $q(\mathbf{r},\mathbf{u},0)=1$.[6,8] Because the two ends of the copolymer are distinct, a second distribution function, $q^\dagger(\mathbf{r},\mathbf{u},s)$, is introduced with a nearly identical definition except that the functional integration over $\mathbf{r}_\alpha(t)$ is done for $t=s$ to 1. It satisfies $q^\dagger(\mathbf{r},\mathbf{u},1)=1$, and Eq. (14) with the right-hand side multiplied by -1. In terms of these end-segment distribution functions, the A-segment density, Eq. (8), is expressed as

$$\phi_A(\mathbf{r})=\frac{4\pi V}{\mathscr{Q}}\int_0^f ds\int d\mathbf{u}q(\mathbf{r},\mathbf{u},s)q^\dagger(\mathbf{r},\mathbf{u},s). \tag{15}$$

The expression for $\phi_B(\mathbf{r})$ is analogous.

When dealing with periodically ordered structures, it is advantageous to express the above equations in terms of a basis function expansion. In doing so, a function $g(\mathbf{r},\mathbf{u})$ is expanded as

$$g(\mathbf{r},\mathbf{u})=\sum_i g_i f_i(\mathbf{r},\mathbf{u}), \tag{16}$$

where the basis functions, $f_i(\mathbf{r},\mathbf{u})$ for $i=1,2,3,\ldots$, are chosen such that they are orthonormal and eigenfunctions of the two Laplacian operators;

$$\frac{1}{4\pi V}\int d\mathbf{r}d\mathbf{u} f_i(\mathbf{r},\mathbf{u})f_j(\mathbf{r},\mathbf{u})=\delta_{ij}, \tag{17}$$

$$\nabla_u^2 f_i(\mathbf{r},\mathbf{u})=-\ell_i(\ell_i+1)f_i(\mathbf{r},\mathbf{u}), \tag{18}$$

$$\nabla_r^2 f_i(\mathbf{r},\mathbf{u})=-\left(\frac{2\pi n_i}{D}\right)^2 f_i(\mathbf{r},\mathbf{u}), \tag{19}$$

where D is the period of the ordered phase. [We adopt a convention where the first basis function is chosen to be $f_1(\mathbf{r},\mathbf{u})=1$ with $n_1=\ell_1=0$.] In this representation, the differential equations for the end-segment distribution functions become

$$\frac{dq_i(s)}{ds}=\begin{cases}\sum_j A_{ij}q_j(s), & \text{if } s<f,\\ \sum_j B_{ij}q_j(s), & \text{if } f<s,\end{cases} \tag{20}$$

$$\frac{dq_i^\dagger(s)}{ds}=\begin{cases}-\sum_j q_j^\dagger(s)A_{ji}, & \text{if } s<f,\\ -\sum_j q_j^\dagger(s)B_{ji}, & \text{if } f<s,\end{cases} \tag{21}$$

where

$$A_{ij}=-\frac{bN}{D}\Lambda_{ij}-\frac{N}{2\kappa}\ell_i(\ell_i+1)\delta_{ij}-\sum_k w_{A,k}\Gamma_{ijk}, \tag{22}$$

$$B_{ij}=-\frac{bN}{D}\Lambda_{ij}-\frac{N}{2\kappa}\ell_i(\ell_i+1)\delta_{ij}-\sum_k w_{B,k}\Gamma_{ijk}, \tag{23}$$

$$\Lambda_{ij}=\frac{D}{4\pi V}\int d\mathbf{u}\mathbf{u}\cdot\int d\mathbf{r} f_i(\mathbf{r},\mathbf{u})\nabla_r f_j(\mathbf{r},\mathbf{u}), \tag{24}$$

$$\Gamma_{ijk}=\frac{1}{4\pi V}\int d\mathbf{r}d\mathbf{u} f_i(\mathbf{r},\mathbf{u})f_j(\mathbf{r},\mathbf{u})f_k(\mathbf{r},\mathbf{u}). \tag{25}$$

We note that Γ_{ijk} is a symmetric tensor, and that Λ_{ij} is antisymmetric.[12] Because $q_i(s)$ and $q_i^\dagger(s)$ are solutions of first-order linear differential equations with $q_i(0)=q_i^\dagger(1)=\delta_{i1}$, they can be expressed analytically;

$$q_i(s)=\begin{cases}T_{A,i1}(s), & \text{if } s<f,\\ \sum_j T_{B,ij}(s-f)T_{A,j1}(f), & \text{if } f<s,\end{cases} \tag{26}$$

$$q_i^\dagger(s)=\begin{cases}\sum_j T_{B,1j}(1-f)T_{A,ji}(f-s), & \text{if } s<f,\\ T_{B,1i}(1-s), & \text{if } f<s,\end{cases} \tag{27}$$

where $T_A(s)\equiv\exp(As)$ and $T_B(s)\equiv\exp(Bs)$. The matrices, $T_A(s)$ and $T_B(s)$, are each evaluated by performing a linear transformation that diagonalizes the matrix in the exponential function.

Now that the amplitudes of the end-segment distribution functions are known, $\mathcal{Q}$ is given by $4\pi V q_1(1)$, the amplitudes of $\phi_A(\mathbf{r})$ are

$$\phi_{A,i}=\frac{1}{q_1(1)}\int_0^f ds\sum_{jk} q_j(s)q_k^\dagger(s)\Gamma_{ijk}, \tag{28}$$

and the amplitudes of $\phi_B(\mathbf{r})$ are given by a similar expression. These expressions satisfy Eqs. (8) and (9). Because $\xi(\mathbf{r})$ is not required, all that remains to be satisfied is Eq. (10) and the equation obtained by subtracting Eqs. (11) and (12). This is done by adjusting $w_{A,i}$ and $w_{B,i}$ so that

$$\phi_{A,i}=-\phi_{B,i}=(w_{A,i}-w_{B,i})/2\chi N, \tag{29}$$

for each $i>0$ where $\ell_i=0$. Since uniform fields do not affect chain statistics, we are free to set $w_{A,1}=\chi N\phi_{B,1}$ and $w_{B,1}=\chi N\phi_{A,1}$. The free energy in Eq. (6) can now be expressed to within an additive constant as

$$\frac{F}{nk_BT}=-\ln[q_1(1)]-\chi N\sum_i \phi_{A,i}\phi_{B,i}. \tag{30}$$

For the disordered phase, this expression reduces to $F/nk_BT=\chi N f(1-f)$. For a periodic ordered phase, F must be minimized with respect to D.

In this preliminary study, our attention is restricted to the lamellar phase. The basis functions for this phase are chosen as

$$f_i(\mathbf{r},\mathbf{u})=\begin{cases}C_{\ell_i}\mathrm{P}_{\ell_i}(u_z), & \text{if } n_i=0,\\ \sqrt{2}C_{\ell_i}\cos(2\pi n_i z/D)P_{\ell_i}(u_z), & \text{if } \ell_i \text{ even},\\ \sqrt{2}C_{\ell_i}\sin(2\pi n_i z/D)P_{\ell_i}(u_z), & \text{if } \ell_i \text{ odd},\end{cases} \tag{31}$$

where z is the spatial coordinate orthogonal to the lamellae, u_z is the projection of $\mathbf{u}$ onto the z axis, and $C_\ell\equiv\sqrt{2\ell+1}$ is a normalization constant. The basis function expansion, in principle, includes all orders (i.e., $\ell_i=0,1,2,\ldots$) of Legendre polynomials, $P_{\ell_i}(u_z)$. For even ℓ_i, the Fourier series expansion is in terms of cosine functions with $n_i=0,1,2,3,\ldots$, and for odd ℓ_i, it is in terms of sine functions with $n_i=1,2,3,\ldots$ The functions become less important as either ℓ_i or n_i increase. To perform a calculation, it is necessary to truncate the set of basis functions. Starting with a small set of the most relevant basis functions, we examine F and D as the number of functions is increased, and stop

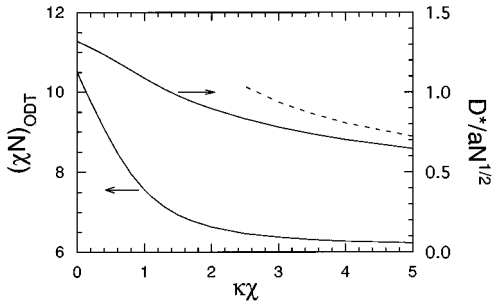

FIG. 1. Order–disorder transition $(\chi N)_{\mathrm{ODT}}$ (lower solid curve) and period of the instability D^* (upper solid curve) as a function of molecular rigidity $\kappa\chi$. The dashed curve represents the asymptotic $(\kappa\chi\to\infty)$ behavior, $D^*\sim 0.91bN$. In the same limit, $(\chi N)_{\mathrm{ODT}}$ approaches 6.135.

once convergence is achieved. In general, increasing χN requires the expansion to include larger n_i, and increasing $\kappa\chi$ requires larger ℓ_i.

III. RESULTS

The present study examines fully symmetric diblocks with $f=1/2$, $b_A=b_B\equiv b$, and $\kappa_A=\kappa_B\equiv\kappa$. These diblocks can only exhibit either a disordered phase or a lamellar microstructure. Within mean-field theory, the order–disorder transition (ODT) between these states is continuous (i.e., second-order). For Gaussian chains, the ODT occurs at $\chi N=10.495$ with an instability at a wavelength of $D^*=1.32aN^{1/2}$.[13] As the rigidity is increased, the ODT moves to lower χN and the instability shifts to smaller $D^*/aN^{1/2}$, as illustrated in Fig. 1. The decrease in $(\chi N)_{\mathrm{ODT}}$ can be attributed to a reduction in the conformational entropy of the molecules, since configurations with sharp bends are unlikely to occur for stiff polymers. This enhances the relative importance of the enthalpy contribution to the free energy, which favors the ordered state. As $\kappa\chi\to\infty$ and the molecules become rigid rods, the transition asymptotically approaches $(\chi N)_{\mathrm{ODT}}=6.135$, and the wavelength of the instability scales linearly with molecular weight as $D^*=0.91bN$.

The ordered state of the block copolymer is characterized by two lengths, its domain spacing D, and the width w, of its internal interface. Here, we define the interfacial width of the lamellar phase as

$$w=\left|\frac{d}{dz}\phi_A(z)\right|^{-1}_{z=z_0}, \tag{32}$$

where $\phi_A(z_0)=1/2$. For convenience, these lengths are reduced to dimensionless quantities by dividing them by a length characteristic to the molecule. For a Gaussian chain, it is natural to use its rms end-to-end length $aN^{1/2}$, and for a rigid molecule, its contour length bN is appropriate. For a semiflexible chain, there is a slight dilemma over which to choose, because the choice can affect how the results are viewed. In Fig. 2, this is illustrated by comparing the A-segment profile of two strongly segregated $(\chi N=60)$ lamellar microstructures, one with stiff chains $(\kappa\chi=6.0)$ and another with relatively flexible chains $(\kappa\chi=0.6)$. When plotted in terms of bN, the more rigid polymer appears to have larger domains, and in units of $aN^{1/2}$, the opposite effect is created. The first case is intuitive, as a chain becomes more rigid it straightens out causing D to increase. In the second case, imagine that as κ is increased, b is decreased so as to keep $a=b(2\kappa)^{1/2}$ constant; the combination produces a slight decrease in D. For our study, it is more convenient to express lengths in terms of $aN^{1/2}$, primarily because we are interested in comparisons to the Gaussian chain $(\kappa=0)$. Furthermore, Gaussian chains have an infinite contour length, which makes it inappropriate to use the bN length scale in that limit.

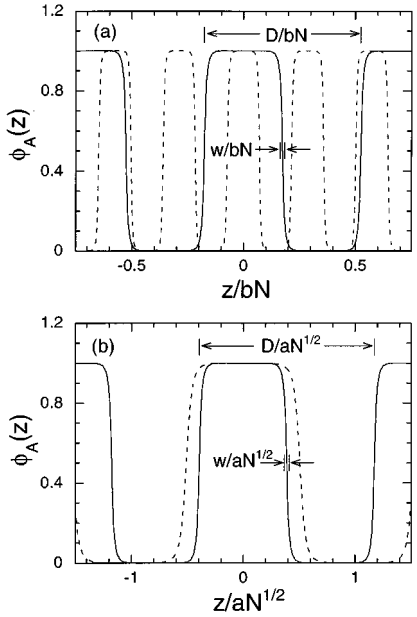

FIG. 2. A-segment profiles of the lamellar phase for $\chi N=60$ with $\kappa\chi=6.0$ (solid curves) and $\kappa\chi=0.6$ (dashed curves). The period D and interfacial width w are indicated for the $\kappa\chi=6.0$ profiles. In (a), distances are measured in units of the contour length bN, and in (b), they are in terms of $aN^{1/2}$, where $a=b(2\kappa)^{1/2}$ is the statistical segment length.

In the strong-segregation limit $(\chi N\gg 10)$, the interfacial width becomes small relative to the domain spacing. Once the molecular weight becomes large $(N\gg\kappa)$, both lengths are expected to scale with exponents that are independent of the actual microstructure. To illustrate this scaling, Fig. 3 provides logarithmic plots of D and w for three degrees of molecular rigidity. The dashed lines denote the slopes corresponding to strong-segregation scaling (i.e., $D\sim a\chi^{1/6}N^{2/3}$ and $w\sim a\chi^{-1/2}$). The results indicate that these degrees of rigidity do not affect the scaling exponents. However, the proportionality constants are clearly affected.

Semenov[14] has examined strongly segregated interfaces for small degrees of molecular rigidity. He showed that the rigidity reduces the tension and width of the internal interface by factors of $(1-\frac{3}{20}\kappa\chi)$ and $(1-\frac{9}{20}\kappa\chi)$, respectively. Because the domain spacing is proportional to the one-third power of the interfacial tension, it will be reduced by a factor of $(1-\frac{1}{20}\kappa\chi)$. The ratio w/D decreases by $(1-\frac{2}{5}\kappa\chi)$, and

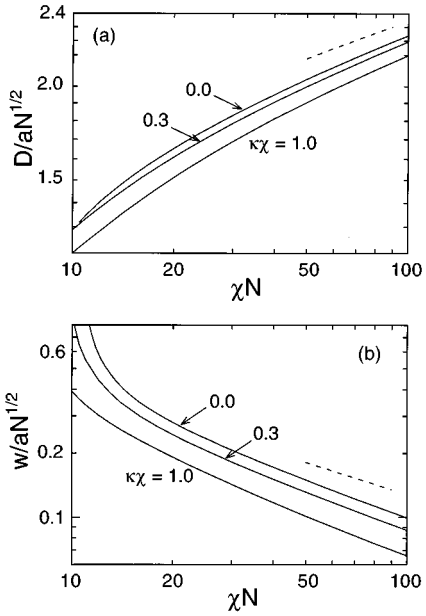

FIG. 3. Logarithmic plots of the (a) lamellar spacing D and (b) interfacial width w as a function of segregation χN for three degrees of molecular rigidity, $\kappa\chi = 0.0$, 0.3, and 1.0. Dashed lines denote slopes consistent with strong-segregation scaling, $D \sim a\chi^{1/6}N^{2/3}$ and $w \sim a\chi^{-1/2}$.

thus increasing $\kappa\chi$ enhances the segregation consistent with the effect on the ODT in Fig. 1, the comparison of the two profiles in Fig. 2, and results below. The decrease in $D/aN^{1/2}$ and $w/aN^{1/2}$ for semiflexible chains with respect to $D_G/aN^{1/2}$ and $w_G/aN^{1/2}$ for Gaussian chains is examined in Fig. 4 as the molecular bending rigidity of the former is increased. At small $\kappa\chi$, our results behave consistently with

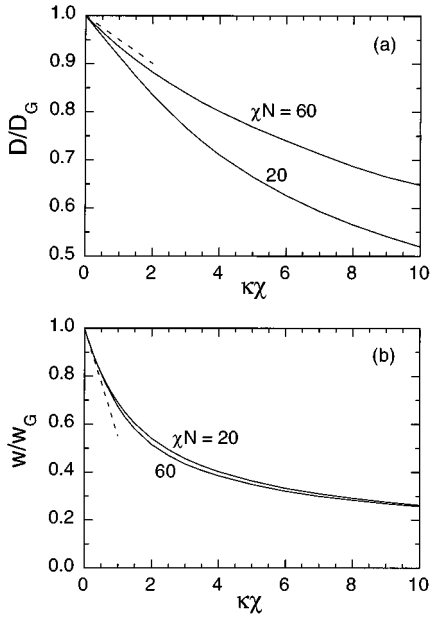

FIG. 4. Plots of the (a) lamellar spacing D and (b) interfacial width w as a function of molecular rigidity $\kappa\chi$ for two degrees of segregation, $\chi N = 20$ and 60. Dashed lines correspond to $D/D_G = 1 - \frac{1}{20}\kappa\chi$ and $w/w_G = 1 - \frac{9}{20}\kappa\chi$, where D_G and w_G correspond to Gaussian chains.

the prediction of Semenov (the dashed lines). The plots of w/w_G versus $\kappa\chi$ are remarkably independent of χN. Notably, the ratio w/w_G approaches an asymptotic limit of about 0.2 as $\kappa\chi$ becomes of order 10 and the polymer becomes rigid on the length scale of the interfacial width. The curves of D/D_G versus $\kappa\chi$ show a greater dependence on χN with a steeper decrease in D/D_G for the less segregated melts. In the asymptotic limit where $\kappa\chi$ becomes large relative to χN and the molecules become rigid rods, the curves in Fig. 4(a) will decrease as $D/D_G \sim (\kappa\chi)^{-1/2}$.

A nice feature of the SCFT is that it yields the distribution function for each segment. The distribution function for the segment at s along the chain in terms of position $\mathbf{r}$ and orientation $\mathbf{u}$ is

$$d(\mathbf{r},\mathbf{u},s) = \frac{4\pi V}{\mathcal{Q}} q(\mathbf{r},\mathbf{u},s) q^{\dagger}(\mathbf{r},\mathbf{u},s)$$

$$= \frac{1}{q_1(1)} \sum_{ijk} q_i(s) q_j^{\dagger}(s) \Gamma_{ijk} f_k(\mathbf{r},\mathbf{u}). \tag{33}$$

In the Gaussian ($\kappa \to 0$) limit, the flexibility of the chain is so great that $d(\mathbf{r},\mathbf{u},s)$ remains uniform in $\mathbf{u}$ regardless of how strong the fields are that may try to orient it. However, for realistic molecules, any finite $\kappa\chi$ will produce a nontrivial orientational distribution. Naturally, diblocks associated with a particular interface will orient with their A blocks toward the A domain and their B blocks in the opposite direction. With our present sign convention, junctions ($s = 0.5$) in the interfacial region will prefer the orientation where $\mathbf{u}_\alpha(s)$ points to the B domain.

Figure 5 shows the distribution of segments in a lamellar microstructure at $\chi N = 60$ and $\kappa\chi = 0.6$. Here, each diblock is 100 persistence lengths long. The plots of $d(z,u_z,s)$ for $s = 0.5$, 0.75, and 1.0, correspond to the junction, midway along the B block, and the B end of the molecule, respectively. Figure 6 provides similar plots for a much more rigid molecule, $\kappa\chi = 6.0$, that is only 10 persistence lengths long. At this degree of segregation ($\chi N = 60$), the junctions are highly localized at the interface. Although this localization does increase slightly with $\kappa\chi$, the main effect of rigidity is to enhance the orientational order of the junction. As the molecule is traversed toward either end, the order decreases. This is illustrated in Fig. 7 where $d(z,1,s)$ is plotted for a series of steps in s for the two conditions examined in Figs. 5 and 6. In Fig. 7(a), the steps are 5 persistence lengths, and with each step the peak decays by a factor of about 2, which is much smaller than the factor of e^5 expected for unperturbed chains. This slow decay is attributed to forces normal to the interface associated with both the compressibility constraint and the gradient in $\phi_A(z)$, pulling the chains towards the middle of the domains. The secondary peaks visible in Fig. 7(a) represent junctions at the adjacent interface ($z/D = 0.75$), where the $u_z = 1$ orientation is least favorable. The fact that the two peaks for the $s = 0.65$ curve are similar in magnitude reflects the near absence of orientational order. It is interesting to note in Fig. 6(b) that when the middle of a B block ($s = 0.75$) is near an interface, it prefers a parallel

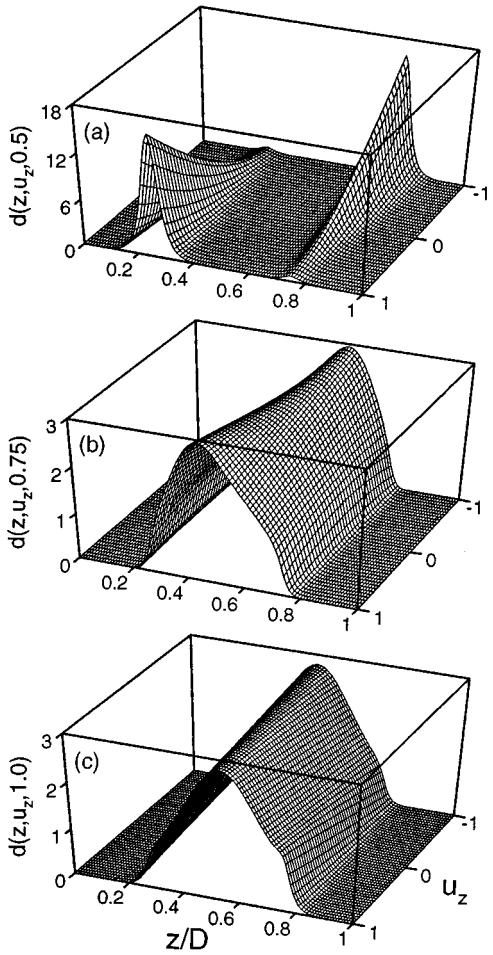

FIG. 5. Segment distributions, $d(z,u_z,s)$, at $\kappa\chi=0.6$ and $\chi N=60$ for the (a) $s=0.5$, (b) $s=0.75$, and (c) $s=1.0$ segments. Note that the scale of the vertical axis varies between plots.

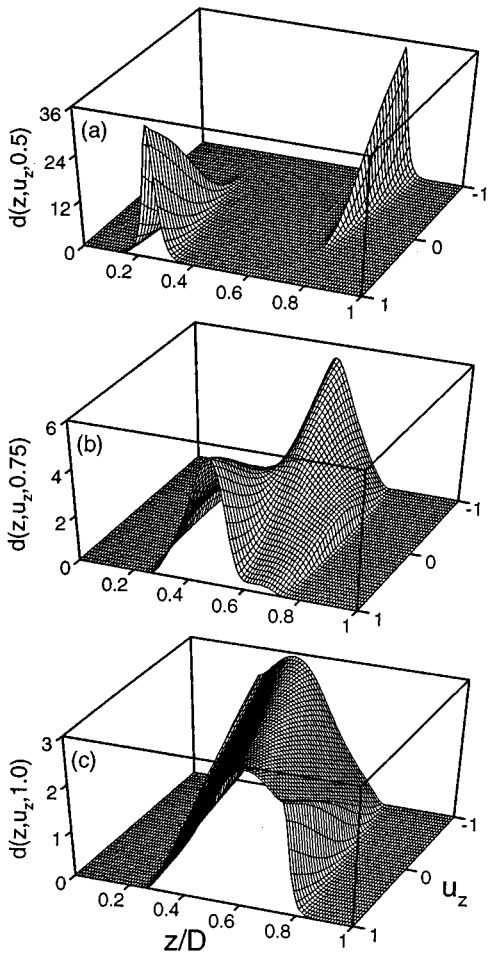

FIG. 6. Segment distributions, $d(z,u_z,s)$, at $\kappa\chi=6.0$ and $\chi N=60$ for the (a) $s=0.5$, (b) $s=0.75$, and (c) $s=1.0$ segments. Note that the scale of the vertical axis varies between plots.

orientation (i.e., $u_z\approx 0$), consistent with calculations for immiscible semiflexible homopolymers.[6]

IV. CONCLUSIONS

We have examined the lamellar phase of semiflexible symmetric diblock copolymers using the wormlike chain model and self-consistent-field theory. This study finds that the order–disorder transition (ODT) shifts towards the disordered state (i.e., smaller χN) with increasing molecular rigidity due to the loss of conformational entropy. In the rigid-rod limit, the ODT occurs at $\chi N=6.135$ and the wavelength of the instability scales with the molecular weight of the molecule, $D^*=0.91bN$. In the ordered state, our results illustrate that moderate molecular rigidities (i.e., $\kappa\chi\sim 1$) do not alter the exponents describing how the domain spacing D and interfacial width w scale with N and χ. However, the proportionality constants are affected. For the lamellar phase at small $\kappa\chi$ and large χN, our results are consistent with strong-segregation predictions,[14]

$$\frac{D}{aN^{1/2}}=2\left(\frac{8}{3\pi^4}\right)^{1/6}\left(1-\frac{1}{20}\kappa\chi\right)(\chi N)^{1/6}, \tag{34}$$

$$\frac{w}{aN^{1/2}}=\frac{2}{6^{1/2}}\left(1-\frac{9}{20}\kappa\chi\right)(\chi N)^{-1/2}. \tag{35}$$

For semiflexible diblocks with a moderate molecular rigidity, the junctions are highly oriented at the interface. This orientational order decays towards both ends of the chain, but typically extends many persistence lengths from the junction.

Most of the results presented here for the lamellar microstructure apply equally to the other block copolymer microstructures. In each case, their stability will increase relative to the disordered state causing the entire ODT to shift to smaller χN with increasing molecular rigidity. We have not considered fluctuation effects that become important near the ODT for low molecular weights, shifting the ODT to larger χN.[4] In each ordered phase, molecular rigidity will lower the interfacial tension, reducing the domain spacing and interfacial width. Since each ordered phase will experience a similar reduction in tension, their relative stabilities will be largely unaffected. Nevertheless, molecular rigidity could change the phase diagram, since the complex structures between the lamellar and hexagonal cylinder ones are so closely matched in free energy.[3] At large rigidities, packing

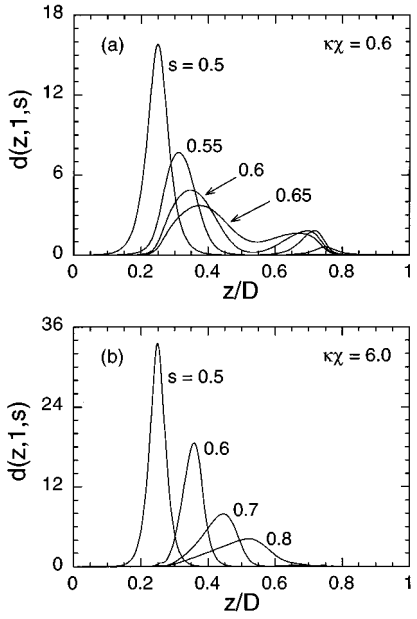

FIG. 7. Segment distributions for **u** aligned with the lamellar normal at (a) $\kappa\chi = 0.6$ and $\chi N = 60$, and at (b) $\kappa\chi = 6.0$ and $\chi N = 60$. In plot (a), each step in s corresponds to five persistence lengths, and in (b), each step is one persistence length.

frustration will become increasingly important, and phase behavior will certainly be altered. Presumably, the phase behavior will evolve from that characteristic of block copolymers to that of thermotropic liquid crystals. Our future work will explore these issues.

The segment interactions in our present calculation are isotropic. One clear advantage of the wormlike chain model over the Gaussian one is that it can be easily extended to include orientational interactions, so as to account for real anisotropies in the segment interactions as well as packing effects which favor parallel arrangements between neighboring segments. Potentially, such interactions could cause the blocks in an ordered microstructure to undergo a transition from Gaussian- to nematic-like configurations producing a discontinuous jump in an appropriate nematic order parameter.[15] Recent experiments have yielded results that appear consistent with such a transition,[16] stimulating us to extend this present work to incorporate orientational interactions. The results will be published in a forthcoming paper.

ACKNOWLEDGMENTS

We are grateful for the suggestions and encouragement provided by F. S. Bates and for a critical reading of the manuscript by G. H. Fredrickson. This work has been supported by the University of Minnesota Supercomputer Institute and by the National Science Foundation through a grant (DMR 94-05101) to F. S. Bates.

[1] F. S. Bates and G. H. Fredrickson, Annu. Rev. Chem. **41**, 525 (1990); F. S. Bates *et al.*, Faraday Discuss. **98**, 7 (1994).
[2] E. Halfand, J. Chem. Phys. **62**, 999 (1975).
[3] M. W. Matsen and F. S. Bates, Macromolecules **29**, 1091 (1996).
[4] G. H. Fredrickson and E. Helfand, J. Chem. Phys. **87**, 697 (1987); J.-L. Barrat and G. H. Fredrickson, *ibid.* **95**, 1281 (1991); A. M. Mayes and M. Olvera de la Cruz, *ibid.* **95**, 4670 (1991); M. Muthukumar, Macromolecules **26**, 5259 (1993).
[5] C. Singh, M. Goulin, A. J. Lui, and G. H. Fredrickson, Macromolecules **27**, 2974 (1994).
[6] D. C. Morse and G. H. Fredrickson, Phys. Rev. Lett. **73**, 3235 (1994).
[7] K. Takahashi and Y. Yunoki, J. Phys. Soc. Jpn. **22**, 219 (1967).
[8] F. Schmid and M. Müller, Macromolecules **28**, 8639 (1995).
[9] A. N. Semenov, Sov. Phys. JETP **61**, 733 (1985).
[10] M. W. Matsen and M. Schick, Phys. Rev. Lett. **72**, 2660 (1994).
[11] O. Kratki and G. Porod, Rec. Trav. Chim. **68**, 1106 (1949).
[12] Using the chain rule and noting that spatially dependent basis functions are sinusoidal, it immediately follows that the integral for $\Lambda_{ij}+\Lambda_{ji}$ is zero. Hence, Λ_{ij} is antisymmetric.
[13] L. Leibler, Macromolecules **13**, 1602 (1980).
[14] A. N. Semenov, Macromolecules **26**, 6617 (1993).
[15] D. R. M. Williams and A. Halperin, Phys. Rev. Lett. **71**, 1557 (1993).
[16] A. J. Ryan (private communication).